A. M. Steinberg, I. Boxx, C. M. Arndt, J. H. Frank, and W. Meier, Experimental study of flame-hole reignition mechanisms in a turbulent non-premixed jet flame using sustained multi-kHz PIV and crossed-plane OH PLIF, Proceedings of the Combustion Institute 33 (2011) 1663-1672.

Original publication available at www.elsevier.com

http://dx.doi.org/10.1016/j.proci.2010.06.134

Experimental study of flame-hole reignition mechanisms in a turbulent non-premixed jet flame using sustained multi-kHz PIV and crossed-plane OH PLIF

A. M. Steinberg[a], I. Boxx[a], C. M. Arndt[a], J. H. Frank[b], and W. Meier[a]

[a] *Institut für Verbrennungstechnik, Deutsches Zentrum für Luft- und Raumfahrt (DLR), 70569 Stuttgart, Germany*
[b] *Combustion Research Facility, Sandia National Laboratories, Livermore, CA, 94551, USA*

Abstract

The dynamics of flame-hole reignition were studied experimentally in a turbulent non-premixed $CH_4/H_2/N_2$ jet flame at $Re_d = 22,800$ (flame 'DLR-B' from the TNF workshop). Simultaneous measurements of the OH combustion radical and velocity field were performed using planar laser induced fluorescence (PLIF) and particle image velocimetry (PIV) at a sustained rate of 10 kHz. The dynamics of the reignition process were tracked through time and two reignition mechanisms were identified. Particular care was made to reduce the influence of out-of-plane motion on the analyzed events by simultaneously measuring the OH distribution in crossed planes. Flame-holes reignited due to both edge-flame propagation and turbulent transport of burning flame segments. However, the edge-flame propagation mechanism was dominant and accounted for over 90% of the flame hole reignition rate on average. Furthermore, the presence of large scale turbulent structures adjacent to a flame-hole did not necessarily result in reignition due to turbulent transport. Instead, the edge flames propagated around the perimeter of such structures, indicating intervening regions of well mixed gas. The range of measured edge flame propagation speeds agreed well that of highly-preheated premixed flames, with a mode of approximately 4 m/s and a mean of approximately 7 m/s.
Published by Elsevier, *Proceedings of the Combustion Institute*, 33 (2011) 1663-1672

Keywords: Turbulent flames; Flame extinction; Edge-flames; High-speed diagnostics; Flame-vortex interaction

1. Introduction

The interaction of turbulence with a non-premixed flame can cause a local deviation from thermal equilibrium in which the rate of heat transport away from the flame surface due to turbulent diffusion exceeds the rate of heat release from the chemical reactions. Such a state can lead to local extinction of the flame surface and can be recognized by the coincidence of high scalar dissipation rate layers with the stoichiometric contour [1–5]. After the onset of extinction, the edge-flames at the hole perimeter act as an extinction front and the flame-hole grows with time. This growth does not however continue indefinitely and at some point the flame-hole begins to reignite [2, 3, 5–8]. Extinction and reignition events such as these negatively affect the stability, combustion efficiency, and pollutant emission characteristics of practical combustion devices.

Two mechanisms of flame-hole reignition are generally described. Firstly, local premixing of the fuel and oxidizer occur at the site where the flame is extinguished. The extinction front at the hole edge may then transition to an ignition front and propagate inwards along the stoichiometric mixture-fraction iso-surface [2, 3, 6–8]. Reignition due to edge-flame propagation has been studied extensively for flame-holes in laminar counter-flow flames perturbed by simple vortices [8–10]. It has been found that edge-flames propagate against the flow at speeds comparable to those of a freely propagating laminar flame. However, the transition from an extinction front to a propagating edge-flame and the subsequent hole reignition are necessarily more complex in a fully turbulent flame than in a laminar flame. Turbulent mixing will affect the rate at which the transition occurs. The premixed edge-flame will then propagate into a turbulent flow, which will affect its speed and dynamics. To date, very few studies of edge-flames dynamics in turbulent flows have been performed [7].

A flame-hole also may recover due to turbulent transport of heat and species across mixture fraction iso-surfaces. That is, the turbulent flow may transport one burning flame segment to another, resulting in a single continuous flame. The edge-flames in this case move with the flow and do not necessarily propagate into it. Flame-hole reignition due to this mechanism has been reported in Direct Numerical Simulations (DNS) of turbulent non-premixed flames [2, 3, 5]. However, this mechanism does not occur in laminar counter-flow flame/vortex configurations and has not been conclusively demonstrated experimentally in turbulent flames [7].

It is therefore necessary to perform detailed studies of flame-hole reignition in fully turbulent flames. In the present work, simultaneous measurements of the OH combustion rad-

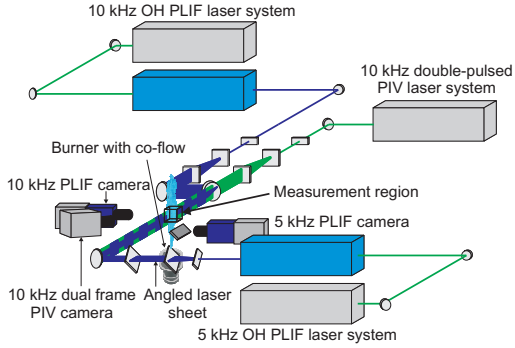

(a) Diagnostics layout

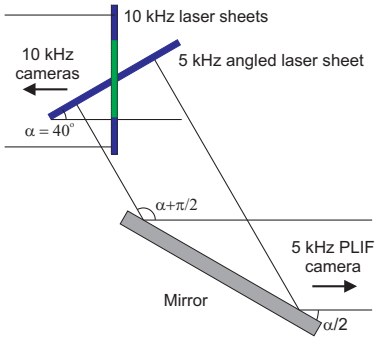

(b) Angled sheet geometry

Fig. 1: Schematic of the simultaneous multi-kHz PIV and crossed-plane OH PLIF diagnostics

ical and velocity field were performed in a turbulent non-premixed jet flame using simultaneous planar laser induced fluorescence (PLIF) and particle image velocimetry (PIV) at a sustained repetition rate of 10 kHz. Particular care was taken to reduce the influence of out-of-plane motion on the analyzed reignition events by simultaneously observing the OH distribution in crossed planes. This allowed the dynamics of both above mentioned flame-hole reignition mechanisms to be experimentally observed and quantified.

2. Experiment and diagnostics

2.1. Burner

The flame studied corresponds to target flame 'DLR-B' from the TNF workshop [11]. A fuel stream comprised of 22.1% CH_4, 33.2% H_2, and 44.7% N_2 issued from a tube with an inner diameter of $d = 8$ mm into a coflowing air stream. The mean jet exit velocity was 63.2 m/s, corresponding to a Reynolds number of $Re_d = 22,800$, and the coflow velocity was 0.3 m/s. All flow rates were measured using calibration standard Coriolis flow meters (Siemens Sitrans F C). The flame was close to the blow-off limit and exhibited frequent local extinction and reignition events. All of the measurements presented below were obtained with a field-of-view centered at an axial location of $x/d = 10$.

Extensive characterization of this flame previously has been performed [12–15], making it an appropriate configuration for validation of turbulent combustion models. In this study, the DLR-B flame was seeded with titanium dioxide particles to enable the velocity measurements. To verify that heat transfer to the particles did not affect the extinction characteristics, the flame-holes statistics for the seeded and unseeded flames were compared by applying the analysis routine described in Section 3 to 7000 OH LIF images from each flame. The probability distribution functions (PDFs) of the hole size and the number of holes per image were computed for each case and were virtually identical, indicating that heat transfer to the particles had a negligible impact on the extinction characteristics of the DLR-B jet flame.

2.2. Particle image velocimetry

Particle image velocimetry (PIV) was performed at a sustained repetition rate of 10 kHz in a plane parallel to the streamwise flow direction. The system, shown in Fig. 1, consisted of a high-speed, dual-cavity, diode-pumped, solid state Nd:YAG laser (Edgewave, IS6II-DE) and a high-speed CMOS camera (LaVision HSS6). Laser pulse pairs (2.6 mJ/pulse, 532 nm, 9 ns pulse) repeating at 10 kHz were formed into a sheet with a 0.5 mm waist along the jet centerline using three cylindrical lenses. The Mie scattered light from the particle laden flow was collected into the camera using a commercial camera lens (Nikkor, $f = 200$ mm) over 0.7 s data acquisition periods.

The PIV camera was placed at a slightly forward scatter angle in order to accommodate the PLIF camera and to increase the light scattered in the camera direction. The camera body and lens were therefore angled relative to each other in order to maintain focus across the light sheet. The perspective distortion brought about by this configuration was corrected by imaging a three-dimensional dot target (LaVision type 7) that was placed in the measurement plane. The distorted dot target was transformed to a normal coordinate system using the pinhole camera model in the LaVision DaVis 7.2 software package. The same target images were used to align the field-of-view from the PIV camera with those from the PLIF cameras described below.

Vector fields were computed from the particle image spatial cross-correlation using the LaVision DaVis 7.2 software package. An adaptive multi-pass vector evaluation technique was used, with interrogation boxes ranging from 64 pixels to 16 pixels. In dual frame mode at 10 kHz, the PIV camera had an active sensor size of 512 x 512 pixels. The field-of-view imaged by the PIV system was 12 mm x 11 mm, resulting in a spatial resolution and vector spacing of approximately 0.34 mm and 0.17 mm respectively. The final velocity fields were smoothed with a 3 x 3 vector moving average filter for the subsequent analysis.

The temporal spacing between correlated laser pulses (Δt_{PIV}) had to be carefully tuned in order to capture the full range of velocities present in the measurement plane. That is, the flame existed between the high-speed inner jet (63.2 m/s) and the low speed co-flow (0.3 m/s). Velocities within the measurement plane ranged from 1 m/s to 50 m/s, which is a large dynamic range for PIV. Data sets therefore were obtained with Δt_{PIV} ranging from 5 μs to 100 μs. It was found that both extremes of the velocity range could be resolved with $\Delta t_{PIV} = 10$ μs. Furthermore, the flame was located in the region where the mean velocity was approximately 10 m/s, which was very accurately resolved at this value of Δt_{PIV}.

2.3. Planar laser induced fluorescence

Two planar laser induced fluorescence (PLIF) systems were used to image the OH radical in crossed planes. One system operated at 10 kHz and obtained images in a plane that was coincident with the PIV plane (parallel to the streamwise flow). Data from this plane were used to identify and track the flame-holes as they interacted with the velocity field. The second system operated at 5 kHz and imaged a plane that was inclined at 40° from the horizontal. This plane was used to determine the out-of-plane hole geometry and to exclude any holes that exhibited strong out-of-plane motion from the analysis.

Each system consisted of a frequency-doubled diode-pumped solid-state laser (Edgewave IS8II-E) that pumped a dye laser (Sirah Credo - 10 kHz, Sirah Cobra-Stretch HRR - 5 kHz). The output of each dye laser was frequency doubled using BBO crystals and tuned to excite the $Q_1(6)$ line of the A-X (1,0) transition of OH at 282.9 nm, with a final energy of approximately 0.1 mJ/pulse. Each laser beam was expanded through a two-lens cylindrical telescope, creating collimated sheets approximately 40 mm in height, and then contracted to a waist using a third cylindrical lens. However, the lenses used to create the sheet from the 5 kHz laser were rotated about their axis such that the sheet was formed at an angle of 40° from the horizontal as shown in Fig. 1. The 10 kHz PLIF laser sheet was combined with the PIV laser sheet using a dichroic mirror and both were transmitted to the measurement location from the same side of the burner. The 5 kHz laser sheet was transmitted to the measurement location from the opposite side. For the purposes of this analysis, the differential absorption of the PLIF laser sheets as they traversed the flame from opposite sides was not significant.

The OH fluorescence signal in the range of 310 nm was acquired from each plane with CMOS cameras (LaVision HSS5) equipped with external, two-stage, lens-coupled intensifiers (LaVision HS-IRO). The cameras had resolutions of 512 x 512 pixels and 768 x 768 pixels at 10 kHz and 5 kHz, respectively. Fluorescence from the 10 kHz system was collected using a 45 mm, f/1.8 lens (Cerco), while fluorescence from the 5 kHz system was collected using a 100 mm f/2.0 lens (Halle). Background luminosity and elastic scattering from the laser sheets were reduced by using 500 ns intensifier gates and high-transmission (>80% at 310 nm) bandpass interference filters (Laser-Components GmbH). Interference between the signals from each system was prevented by offsetting the laser pulses by 1 μs. Both PLIF laser pulses were centered in the 10 μs delay between PIV laser pulses. The OH images were corrected for non-uniformity in the mean laser sheet intensity profile, determined from a 1000 image ensemble average of fluorescence from a uniform acetone field that was introduced into the test area. A correction also was made to remove the mean flame luminosity. Data was collected over 0.7 s intervals, resulting in approximately 3.4 GB of data from each camera per run. Further details about the hardware used in the PLIF systems can be found in Ref. [16].

A novel aspect of this imaging system was the combination of the vertical and angled measurement planes, which provided insight into the three-dimension structure of the turbulent flame. Previous low-repetition rate studies of the jet flame considered here used ensemble statistics from measurements in a single plane to provide a detailed analysis of the probability of localized extinction and the dimensions of the extinguished regions [14]. Kaminski et al. [17] performed time series PLIF measurements of this jet flame using short bursts of images obtained from a single measurement plane. However, interpretation of such time series measurements is particularly challenging because out-of-plane motion of the three-dimensional turbulent flame structures can produce apparent motion within the measurement plane. The crossed plane measurements in the current study helped to alleviate these ambiguities. Measurements in planes normal to the streamwise flow direction have previously been performed in non-reacting jets and flames by viewing the laser sheet at an oblique angle and enforcing the Scheimpflug criterion between the camera lens and sensor [18, 19]. However, this was not feasible in the current experiment due to the bulk of the high-speed intensifier/camera system. Instead, the out-of-plane hole geometry was imaged in a plane that was inclined by 40° with respect to the horizontal, as described above. The fluorescence signal from this plane was reflected into the collection optics of the 5 kHz camera by a mirror placed below the measurement plane. Using the combination of angles indicated in Fig. 1(b), an undistorted and focused image was obtained by the 5 kHz camera. The mirror was located below the exit of the co-flow nozzle and did not affect the flow field.

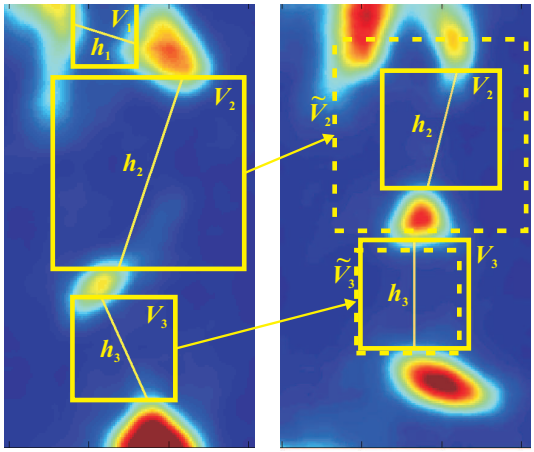

Fig. 2: Demonstration of flame-hole tracking by Lagrangian analysis of the bounding volume around the holes. Flame-holes (h_i) are indicated by the solid lines, the measured bounding volumes (V_i) are indicated by the solid squares, and the predictions for the control volume location based on convection between measurements ($\tilde{V}_i$) are indicated by the dashed squares.

3. Identification and tracking of flame-holes

Flame-holes were identified by the gaps in an otherwise continuous OH layer using the same approach as Kaiser and Frank [14]. The identification and tracking procedure is described for holes in the vertical measurement plane since these are the major focus of the reignition analysis. The OH LIF images were smoothed with a 0.5 mm square filter and converted to binary images using a global threshold. Flame-holes were then identified by the straight line with the minimum length between adjacent OH regions. Incorrect flame-holes (i.e. between non-adjacent OH regions) were removed by selecting the flame-hole combination that connected the islands with the minimum total path length. Mathematically, each flame-hole was treated as a vector,

$$\vec{h}_i(t) = \vec{x}_{i1}(t) + l_i(t)\hat{\xi}_i(t) \quad (1)$$

where $\vec{x}_{i1}$ represents the end of the flame hole closest to the nozzle exit, l_i is the length of the flame-hole, and $\hat{\xi}_i$ is a unit vector pointing along the flame-hole from $\vec{x}_{i1}$ to its opposite end, $\vec{x}_{i2}$.

The flame-holes were tracked through time in a Lagrangian manner (i.e. by following the fluid) using the simultaneous PIV velocity data. Two important tracking abilities were required for this analysis. Firstly, it was necessary to identify the same flame-hole in sequential images. Secondly, it was necessary to track the location and convection of the hole-edges. To identify the same flame-hole through a time sequence, a square control volume ($V_i(t)$) was defined around each detected flame-hole. The mean velocity within $V_i(t)$ was used to estimate the displacement of the control volume between frames:

$$\tilde{V}_i(t_0 + \Delta t) = V_i(t_0) + \overline{\vec{u}}(V_i(t_0), t_0)\Delta t \quad (2)$$

where $\tilde{V}_i(t_0+\Delta t)$ represents the estimate for the control volume location at the next measurement time and $\overline{\vec{u}}(V_i(t_0),t_0)$ is the mean velocity in $V_i(t_0)$. However, the velocity field within the control volume changed between frames as the turbulence evolved. This resulted in slightly incorrect displacements based on Eq. 2 that could lead to smaller holes being incorrectly tracked. An iterative procedure therefore was implemented, where the convective velocity of the control volume was taken to be the mean of the velocity field within $V_i(t_0)$ and $\tilde{V}_i(t_0+\Delta t)$. This was repeated until the displacement of $\tilde{V}_i(t_0+\Delta t)$ changed by less than 5% between iterations. The corresponding flame-hole at the next time step, $\vec{h}_i(t_0+\Delta t)$, then was selected to be the flame-hole within the final $\tilde{V}_i(t_0+\Delta t)$. If multiple flame-holes were present in $\tilde{V}_i(t_0+\Delta t)$, the hole that most closely matched the orientation of $\vec{h}_i(t_0)$ was selected. Various additional conditions and checks were implemented to improve the robustness of the tracking method. These included a recursive process that selected the most probable total path for two adjacent flame-holes convecting together (i.e. without the holes jumping each other), and a check to remove new flame-holes (either newly generated or convecting into the measurement plane) from incorrectly being identified as the continuation of a flame-hole from a previous frame.

The results of the tracking procedure are demonstrated in Fig. 2 for a sequence of two images containing three flame-holes. As can be seen, the procedure correctly identified and tracked each hole, eliminating hole h_1 when it exited the measurement area. Visual comparison of the flame-holes tracked by the algorithm and those identified manually indicated that the algorithm correctly selected the flame-hole approximately 90% of the time. Hole identification errors typically occurred in situations where a new flame-hole appeared in the measurement plane adjacent to a previously existing hole. However, such time sequences were rare and often involved out-of-plane convection of holes through the vertical measurement plane. Such sequences were not tractable for the subsequent analysis of flame-hole reignition and were therefore excluded from consideration as described below.

The other aspect of the flame-holes that needed to be tracked through time was the location of the edges, which was a function of the convective velocity and OH production rate. The location to which each hole endpoint, $\vec{x}_{ij}(t)$, would passively transport due to fluid motion was determined using the same iterative procedure that was used for the control volumes. An average of the four velocity measurements in a square around the hole endpoints was used for the convective velocities. The results of the edge-flame convection procedure will be discussed in greater detail in Section 5.

The exact flame-hole geometry was somewhat dependent on the threshold that was used to binarize the OH LIF images. Two threshold levels therefore were tested for comparison, with the second being 25% larger than the first. Although the choice of the threshold signal had a minor effect on the measurements of flame-hole size, the statistics of flame-hole reignition were unaffected. Furthermore, the results from individual extinction events were qualitatively and phenomenologically independent of the threshold. Hence, results from only the lower threshold are presented here.

4. Reduction of out-of-plane convection effects

Out-of-plane convection of the flame-holes could erroneously appear as reignition, or further extinction, due to apparent edge-flame propagation in the vertical measurement plane. To avoid these artifacts in the reignition analysis, the OH LIF signal from the angled measurement plane was used to exclude holes for which out-of-plane convection significantly affected the observed evolution in the vertical measurement plane. Flame-holes were simultaneously imaged in both crossed measurement planes and therefore could be matched to each other based on their temporal and spatial locations. The center of each matched hole in the radial direction then was determined. Appendix A provides a relationship between the hole size, the allowable amount of out-of-plane convection (relative to the hole size), and the apparent rate of edge-flame propagation caused by this convection. Only events for which the apparent reignition rate due to out-of-plane convection was less that 0.15 m/s were included in the subsequent analysis. It is shown in Appendix A that the total uncertainty in the measured edge-flame speed under this restriction is less than 0.4 m/s, which is less than 10% of the measured most probable edge-flame speed. It is noted that the analysis in Appendix A is based on a simplified geometric description of the flame-hole convection. However, even if the actual apparent edge-flame speed due to out-of-plane convection was significantly higher than stipulated by this analysis, it would still be small relative to the measured edge speeds.

5. Results and analysis

A recovering flame-hole was identified by the condition $\partial l_i/\partial t < 0$. Flame-holes were studied only if they were present in both measurement planes for the onset of reignition and at least 0.2 ms after the onset of reignition (3 total frames in the 10 kHz system, 2 total frames in the 5 kHz system). In a typical 7000 frame data set, there were approximately 2500 distinct holes. With the restrictions on the allowable out-of-plane convection and the minimum number of recovering frames, approximately 100 of these were usable for the analysis. Approximately 70% of unconsidered holes were eliminated based on the out-of-plane convection criterion. It is unlikely that this restriction had a large effect on the reignition mechanisms; generally it means that the tangential component of the bulk fluid motion was instantaneously significant relative to the axial component. However selecting holes that reignite for a minimum of 0.3 ms slightly biases the results towards larger holes, which have a greater chance of intersecting the measurement planes for extended periods. Within the range of hole-sizes considered for the full analysis, no statistically significant scale-dependent differences in the reignition mechanisms were observed. Nevertheless, the reported statistics may not apply to the smallest scale flame-holes.

For each hole, $h_i(t)$, at each measurement time, t_{ik}, the location to which the flame-hole endpoints would passively convect was determined as described in Section 3. These points were denoted by $\tilde{x}_{ij}(t_{ik}+\Delta t)$ and the distance between them was denoted $\tilde{l}_i(t_{ik}+\Delta t)$. The difference between $l_i(t_{ik})$ and $\tilde{l}_i(t_{ik}+\Delta t)$ represents the change in flame-hole length due to turbulent transport, conceptually occurring across iso-mixture fraction surfaces, which will be denoted dl_i^c/dt. The difference between $l_i(t+\Delta t)$ and $\tilde{l}_i(t_{ik}+\Delta t)$ represents the change in length due to propagation of one or both edge-flames, conceptually occurring along the stoichiometric mixture fraction iso-surface, denoted by dl_i^p/dt. It is noted that the edge-flame propagation speed should ideally be taken relative to the instantaneous velocity upstream of the edge, whereas the reported edge-flame speeds were measured relative to the temporal and spatial velocity averages over successive instants and at the four velocity measurement points surrounding the edge, respectively. The influence of these averages was determined by performing the reignition analysis using only the single velocity measurement point that was closest to the edge and outside the OH region, and without temporal averaging. Individual reignition events showed moderate variation in the

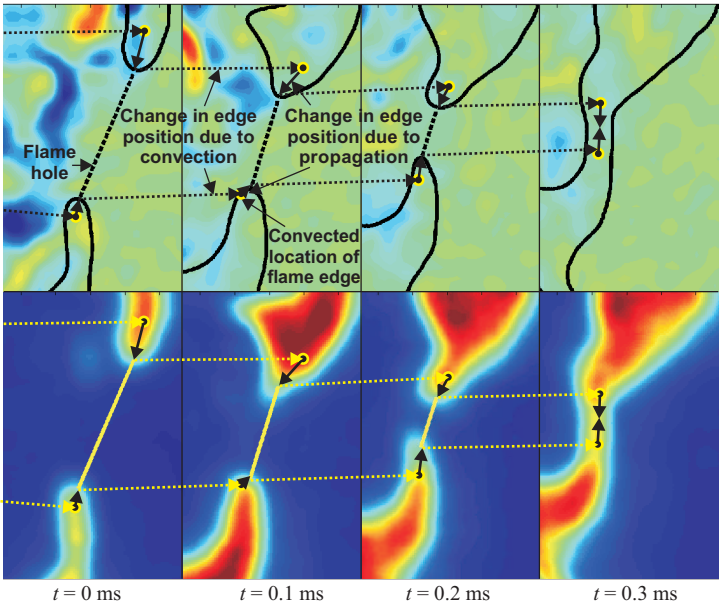

(a) Top sequence - Measured vorticity field (ω_z) between -30000 s^{-1} (blue) and 30000 s^{-1} (red) with OH boundary and flame-hole. Bottom sequence - Measured OH field with flame-hole. In each frame, the locations to which the flame edges had convected are idicated by the dotted-line arrows and circles. The propagation of the edge flames is indicated by the solid-line arrows. The field-of-view is 5 mm x 8 mm.

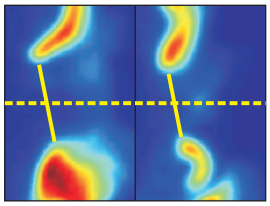

(b) Flame-hole in the angled plane, showing that it did not convect out of the vertical plane.

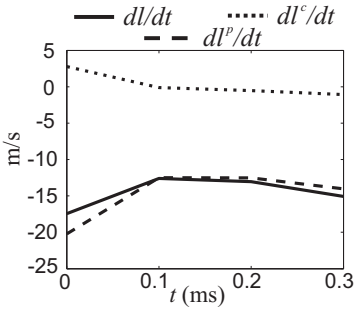

(c) Temporal history of the contribution of each mechanism to the reignition of the flame hole.

Fig. 3: Flame-hole reignition due to edge-flame propagation.

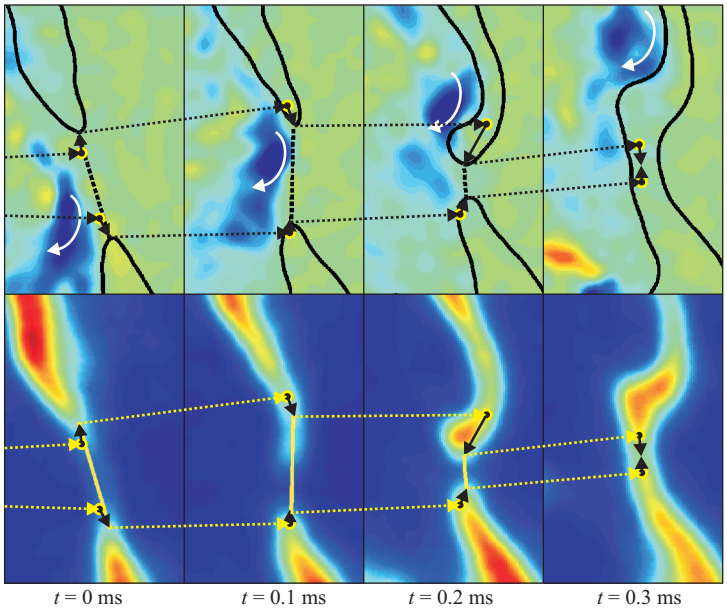

(a) Top sequence - Measured vorticity field (ω_z) between -30000 s^{-1} (blue) and 30000 s^{-1} (red) with OH boundary and flame-hole. Bottom sequence - Measured OH field with flame-hole. In each frame, the locations to which the flame edges had convected are idicated by the dotted-line arrows and circles. The propagation of the edge flames is indicated by the solid-line arrows. The field-of-view is 5 mm x 8 mm.

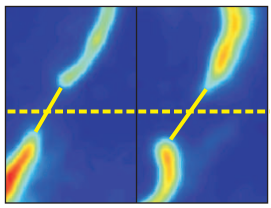

(b) Flame-hole in the angled plane, showing that it did not convect out of the vertical plane.

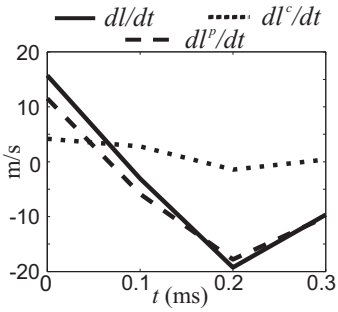

(c) Temporal history of the contribution of each mechanism to the reignition of the flame hole.

Fig. 4: Flame-hole reignition due to edge-flame propagation aided by mixing from an adjacent vortical structure.

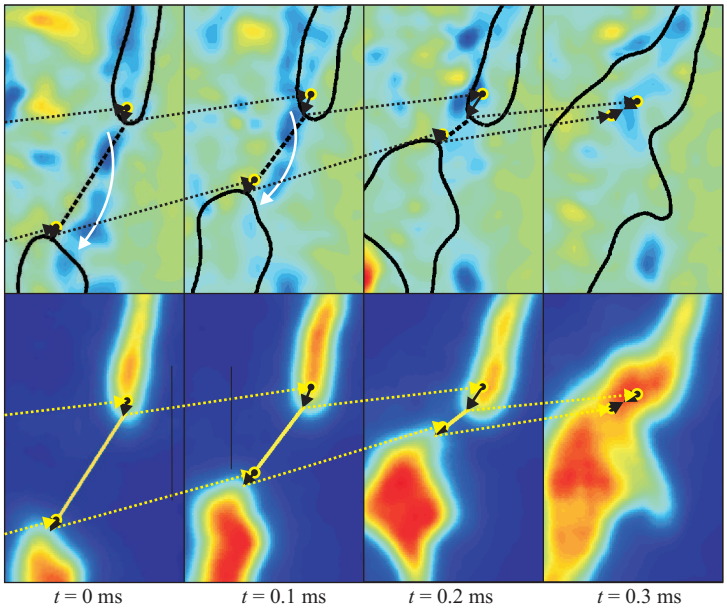

(a) Top sequence - Measured vorticity field (ω_z) between -30000 s^{-1} (blue) and 30000 s^{-1} (red) with OH boundary and flame-hole. Bottom sequence - Measured OH field with flame-hole. In each frame, the locations to which the flame edges had convected are idicated by the dotted-line arrows and circles. The propagation of the edge flames is indicated by the solid-line arrows. The field-of-view is 5 mm x 8 mm.

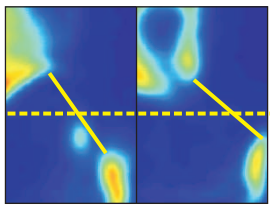

(b) Flame-hole in the angled plane, showing that it did not convect out of the vertical plane.

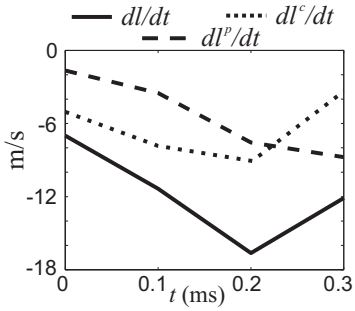

(c) Temporal history of the contribution of each mechanism to the reignition of the flame hole.

Fig. 5: Flame-hole reignition due to a combination of turbulent convection and edge-flame propagation.

reignition rate, dl_i/dt, and the separation into the mechanistic components, dl_i^c/dt and dl_i^p/dt, of up to 15%. However, the phenomenological and statistical results were not significantly altered. The averaging method was used for the final results since it reduced the influence of individual spurious vectors.

Figures 3-5 show three typical flame-hole reignition sequences. Part (a) of each figure shows the reignition event visualized in two different ways. The top sequence shows the vorticity field (ω_z) overlaid with the flame-hole and OH island border. The lower sequence in each figure shows the OH LIF measurements along with the flame-hole. In each frame, the edge motion due to turbulent transport and edge-flame propagation is indicated by the dotted- and solid-line arrows, respectively. The location to which the edge-flame would have been transported by the fluid motion if it was not propagating is indicated by the circles. To the right of these time sequences are OH images from the angled plane with the flame-hole indicated (subfigure (b)). These show that the presented holes did not exhibit significant out-of-plane convection. Finally, the temporal histories of dl_i/dt, dl_i^c/dt, and dl_i^p/dt are shown in subfigure (c).

Figure 3 shows reignition due to simple edge-flame propagation. The edges of the flame-hole propagated straight along the hole line, reigniting the intervening fluid. Figure 3(c) shows that, to within the experimental error, all of the reignition was due to edge-flame propagation. This result was expected since there was no strong turbulent vortical structure adjacent to the hole that could transport the edge-flames towards each other.

More surprisingly, it was found that the presence of a strong vortical structure adjacent to the flame-hole did not generally cause the flame to reignite due to turbulent transport. Instead, an edge-flame rapidly propagated in an arc around the structure, indicating an intervening region with significant fuel/air mixing. Figure 4 shows such an interaction. The first frame in this sequence shows an instant when the edge-flames were extinction fronts; the edge-flames propagated farther apart between measurements. A vortical structure with clockwise rotation existed on the fuel side of the flame and the upper edge-flame rapidly propagated around this structure. Figure 4(c) shows that this reignition event was almost entirely due to edge-flame propagation. It is noted that the location considered as the 'edge' in such cases may not have been exactly at the location of OH production (i.e. in the propagation direction), but was defined as the location that minimized the distance between the separate OH islands. This could provide a slight shift towards lower edge-flame speeds in these situations.

Figure 5 shows one of the few cases where the reignition was largely caused by turbulent transport of burning flame segments. In this time sequence, a long vortical structure helps to convect the upper edge of the flame-hole towards the lower edge. However, Fig. 5(c) shows that edge-flame propagation was still a significant contributor to the overall reignition.

Figure 6 shows the PDF of the rate of flame-hole reignition due to edge-flame propagation relative to the total reignition rate. Approximately 200 interactions were studied to generate this PDF. For each interaction, the temporal history of each reignition mechanism was calculated (similar to subfigure (c) in the above interactions). The PDF was then compiled from the mean contribution of the edge-flame mechanisms to each interaction. As can be seen, edge-flame propagation was responsible for the vast majority of reignition, with a mean contribution of 93% to the total reignition speed. There were several cases where the flame-hole was reigniting due to propagation while the flame edges were being convected apart. Hence, the edge-flames were propagating inward at a rate that exceeded the overall rate of reignition.

It is noted that this PDF is not necessarily a general result for all turbulent diffusion flames. The current data were taken at $x/d = 10$, a location at which the temperature and OH iso-surfaces were wrinkled but smooth [14]. At further downstream locations or in other flames where scalar iso-surfaces are broken apart, there may be an increased probability for

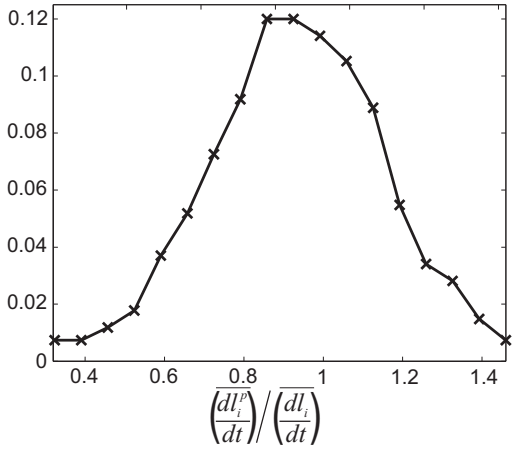

Fig. 6: PDF of the amount of flame-hole recovery due to edge-flame propagation.

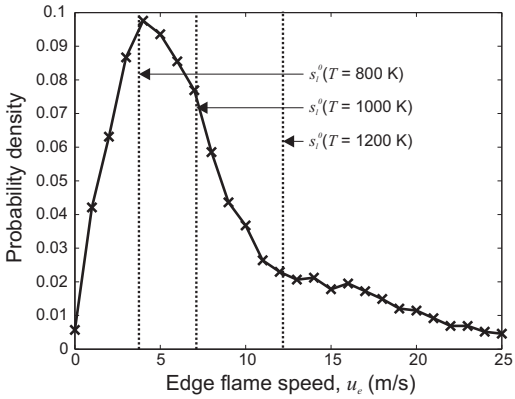

Fig. 7: PDF of the edge-flame propagation speed.

turbulent transport to occur across mixture fraction surfaces to connect burning flame segments. Additional studies at larger x/d locations will investigate this possibility.

The predominance of the edge-flame propagation mechanism was largely due to the high edge-flame propagation speed. Figure 7 shows the PDF of the measured edge-flame speed (u_e). The vertical dashed lines in this figure represent the laminar flame speed (s_l^0) of a stoichiometric mixture of the fuel stream and air at various temperatures as computed by Chemkin using the GRIMech 3.0 chemical mechanism. It was shown in Refs. [14, 20] that the gas in a flame-hole is a mixture of unburnt reactants and hot products at a temperature between that of the fresh gases (approx. 295 K) and that of the adiabatic flame (approx. 2100 K). Hult et al. observed that temperatures of 1000-1200 K were very common in regions without detectable levels of OH[20]. The edge-flames propagate into such hot mixture and therefore are capable of moving at rates far exceeding that of a laminar flame propagating into the unburnt reactants at ambient temperature ($s_l^0(T = 295) = 0.5$ m/s). It is noted that the edge-flames do not propagate into a stoichiometric mixture of pure fuel and air, but an admixture including combustion products. This would affect the theoretical propagation speed of the equivalent premixed flame. Nevertheless, the measured edge-flame speeds corresponded reasonably well to a heated laminar premixed flame. The most probable and mean edge-flame propagation speeds were approximately 4 m/s and 7 m/s respectively, approximately corresponding to the computed laminar flame speeds at 800 K and 1000 K. The highest measured edge-flame speeds are consistent with temperatures in the range of

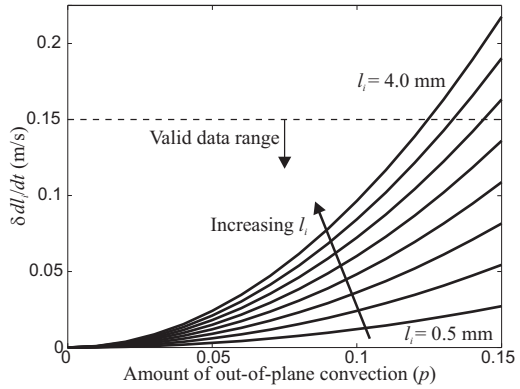

Fig. 8: Error in the apparent edge speed that can be caused by out-of-plane convection.

1400 K, which is below the maximum temperature for which zero-OH levels were observed in this flame [20]. The large range of measured speeds is indicative of different gas temperatures and compositions in the flame-holes.

6. Conclusion

The dynamics of flame-hole reignition were studied experimentally in a turbulent non-premixed jet flame ('DLR-B' from the TNF workshop). The flame was simultaneously imaged in crossed planes using planar laser induced fluorescence of the OH radical, while the velocity field was measured using particle image velocimetry. The measurements were performed at sustained repetition rates of 10 kHz, which allowed the entire flame-hole reignition process to be captured. Reignition occurred by both edge-flame propagation and turbulent convection of burning flame segments. However, the edge-flame propagation mechanism was, on average, responsible for over 90% of the reignition rate. Furthermore, the presence of large scale turbulent structures adjacent to a flame-hole did not necessarily result in reignition by convection. Instead, edge-flames rapidly propagated around the perimeter of these structures, indicating well mixed fuel and oxidizer. The range of measured edge-flame propagation speeds agreed well with those of highly preheated premixed flames, with a mode of approximately 4 m/s and a mean of approximately 7 m/s.

1. Appendix - Error analysis

Potential sources of error in the reported measurements include those due to of out-of-plane hole convection, those in the Lagrangian tracking analysis, and the direct measurement uncertainty. To quantify the influence of out-of-plane convection, one may consider the apparent behavior of a circular hole that is convected through the angled measurement plane while maintaining a constant diameter. Due to the angle of the measurement plane, a circular hole convecting vertically would appear to translate from the side of the sheet with a lower axial location to that with a higher axial location at a speed of $u_h \sin\alpha$, where u_h is the axial convective speed of the hole and α is the sheet angle. The movement of the hole relative to the vertical measurement plane can be determined by subtracting this translation from the measured radial hole dynamics. If the hole is initially centered in the measurement plane and convects a fraction, p, of its diameter out-of-plane between measurements, the apparent rate of change in hole diameter will be:

$$\delta\left(\frac{dl_i}{dt}\right)_o = l_i \frac{1-\left(1-4p^2\right)^{1/2}}{\Delta t} \qquad (3)$$

The notation δ indicates that this is a measurement error and the subscript o indicates that it is due to out-of-plane convection. As mentioned in Section 4, the events studied for this analysis were restricted to those for which $\delta\left(dl_i/dt\right)_o < 0.15$ m/s.

In terms of the observed rate of flame-hole reignition, the major source of error was the out-of-plane convection and $\delta\left(dl_i/dt\right) \approx \delta\left(dl_i/dt\right)_o$. However, additional uncertainty was introduced by the separation of dl_i/dt into its propagative and convective components. The major error in the convective component was due to the first order approximation used to perform the Lagrangian analysis; errors in the actual measured velocities were a negligible contribution. While the iterative procedure employed reduced the error, for the purposes of this analysis, the tracking method will be considered a purely first order approximation. Expanding the displacement in a Taylor series shows that the leading error in the displacement is:

$$\delta\tilde{x}_{ij} = \frac{1}{2}\frac{\partial u}{\partial t}\Delta t^2 \tag{4}$$

Unfortunately, the temporal resolution of the diagnostic was insufficient to accurately resolve the single point acceleration statistics. The mean flow acceleration magnitude at the flame surface was therefore computed based on Taylor's hypothesis as:

$$\overline{\left|\frac{\partial u}{\partial t}\right|} \approx \overline{u}\overline{\left|\frac{\partial u}{\partial x}\right|} \approx 6 \times 10^3 \text{ m/s}^2 \tag{5}$$

Summing the uncertainty from out-of-plane motion with that from the convective approximation in quadrature then yields $\delta\left(dl_i^c/dt\right) = 0.3$ m/s. The propagative component of reignition was the difference between the total reignition rate and the convective component and possessed an uncertainty of $\delta\left(dl_i^p/dt\right) = 0.4$ m/s. There are numerous effects that could cause additional error in the measurements, particularly associated with $\delta\left(dl_i/dt\right)_o$ (for example, non-circular holes). Nevertheless, if the measurement uncertainty was twice that quoted here it would still be less than 25% of the observed most probable reignition rates and edge-flame propagation speeds.

References

[1] N. Peters, *Combust. Sci. Technol.* 30 (1983) 1–17.
[2] P. Sripakagorn, , S. Mitarai, F. Kosály, H. Pitsch, *J. Fluid Mech.* 518 (2004) 231–259.
[3] C. Pantano, *J. Fluid Mech.* 514 (2004) 231270.
[4] J. A. Sutton, J. F. Driscoll, *Proc. Combust. Inst.* 31 (2007) 1487–1495.
[5] J. C. Hewson, A. R. Kerstein, *Combust. Sci. Technol.* 174 (2002) 35–66.
[6] J. Buckmaster, *Prog. Energy Combust. Sci.* 28 (2002) 435–475.
[7] E. Mastorakos, *Prog. Energy Combust. Sci.* 35 (2009) 57–97.
[8] G. Amantini, J. H. Frank, B. A. V. Bennett, M. D. Smooke, A. Gomez, *Combust. Flame* 150 (2007) 292–319.
[9] C. E. Frouzakis, A. G. Tomboulides, J. Lee, K. Boulouchos, *Combust. Flame* 130 (2002) 171–184.
[10] S. Yoo, H. G. Im, *Proc. Combust. Inst.* 30 (2005) 349–356.
[11] *International workshop on measurement and computation of turbulent nonpremixed flames (TNF)*, available from: www.ca.sandia.goc/TNF/.
[12] W. Meier, R. Barlow, Y.-L. Chen, J. Y. Chen, *Combust. Flame* 123 (2000) 326–343.
[13] C. Schneider, A. Dreizler, J. Janicka, E. P. Hassel, *Combust. Flame* 135 (2003) 185–190.
[14] S. A. Kaiser, J. H. Frank, *Proc. Combust. Inst.* 32 (2009) 1639–1646.
[15] J. H. Frank, S. Kaiser, *Exp. Fluids* 44 (2008) 221–233.
[16] I. Boxx, M. Stöhr, C. Carter, W. Meier, *App. Phys. B* 95 (2009) 23–29.
[17] C. Kaminski, J. Hult, M. Aldén, *Appl. Phys. B* 68 (1999) 757–760.
[18] B. Ganapathisubramani, K. Lakshminarasimhan, N. T. Clemens, *J. Fluid Mech.* 598 (2008) 141–175.
[19] A. M. Steinberg, J. F. Driscoll, S. L. Ceccio, *Exp. Fluids* 44 (2009) 985–999.
[20] J. Hult, U. Meier, W. Meier, A. Harvey, C. Kaminski, *Proc. Combust. Inst.* 30 (2005) 701–709.

2. Acknowledgments

Effort sponsored by the Air Force Office of Scientific Research, Air Force Material Command, USAF, under grant number FA8655-08-1-3058. The U.S. Government is authorized to reproduce and distribute reprints for Government purpose notwithstanding any copyright notation thereon. This research also was supported by the U.S. Department of Energy, Office of Basic Energy Sciences, Division of Chemical Sciences, Geosciences, and Biosciences. Sandia National Laboratories is a multiprogram laboratory operated by Sandia Corporation, a Lockheed Martin Company, for the U.S. Department of Energy under contract DE-AC04-94-AL85000.